Supplementary Information for

"Transsynaptic Cerebellin-4/Neogenin-1 Signaling Mediates LTP in the Mouse Dentate Gyrus"

Kif Liakath-Ali[†], Jai S. Polepalli[†*], Sung-Jin Lee, Jean-Francois Cloutier,

and Thomas C. Südhof[*]

*corresponding authors
Emails: jpolepalli@nus.edu.sg; tcs1@stanford.edu)

[†]Equal contributions

This PDF file includes:

Supplementary text (detailed Methods)
Figures S1 to S5
SI References

Supplementary Information Text

METHODS IN DETAIL

Mice. All mouse experiments were performed in accordance with protocols approved by the Administrative Panel on Laboratory Animal Care (APLAC) at Stanford University. *Cbln4* and *Neo1* conditional KO (cKO) mice were previously described (1, 2). *Neo1* cKO mice have LoxP sites flanking the exon 1 of *Neo1* gene. Wild type CD-1 mice were obtained from Charles River Laboratories.

In vivo injections. Postnatal 18-21 day old Cbln4 and Neogenin-1 mice were prepared for stereotaxic injection using standard procedures approved by the Stanford University Administrative Panel on Laboratory Animal Care. AAVs used for in vivo viral injections were obtained from HHMI Janelia Farm viral core facility (3). Briefly, animals were anesthetized with a mixture of ketamine (75 mg/kg body weight) and dexmedetomidine (0.375 mg/kg body weight) by intraperitoneal injection. Following immobilization on a Kopf stereotaxic apparatus, mice were injected bilaterally with AAV virus containing one of hSyn-Cre-eGFP, or hSyn-ΔCre-eGFP. For presynaptic deletion of Cbln-4 from the lateral and medial EC, AAVs containing hSyn-Cre-eGFP, or hSyn-ΔCre-eGFP were injected bilaterally at coordinates -3.6 mm posterior, - 4.2 mm lateral to bregma at a depth of -3.6 mm, and -4.5 mm posterior, - 3.3 mm lateral to bregma at a depth of -3.6 respectively (4). For dentate gyrus in Neogenin-1 cKO mice, AAV virus containing one of hSyn-Cre-eGFP, or hSyn-ΔCre-eGFP were injected bilaterally at -1.6 mm posterior, -1.4 mm lateral to bregma at a depth of -1.8 to -2 mm and at -2 mm posterior, -1.5 mm lateral to bregma at a depth of -1.8 to -2 mm (5), at 4 sites in total to cover the entire dentate gyrus. Viral solution (0.4 µl) in a glass cannula was injected at each site using a microinjection pump (Harvard Apparatus) at a flow rate of 0.1 µl/min in each hemisphere sequentially. The scalp was sealed with cyanoacrylate and atipamezole was injected (10 mg/kg body weight i.p.) to reverse the effect of dexmedetomidine.

Slice electrophysiology. As described (6), ten to fifteen days following the injection of AAV virus, animals were anesthetized with halothane and the brains rapidly removed and placed in ice-cold, high sucrose cutting solution containing (in mM): 228 sucrose, 26 $NaHCO_3$, 11 glucose, 2.5 KCl, 1 NaH_2PO_4, 7 $MgSO_4$ and 0.5 $CaCl_2$. 300 µm sections were cut on a Leica vibratome in the high sucrose cutting solution, and immediately transferred to an incubation chamber containing artificial cerebrospinal fluid (ACSF) containing (in mM) 119 NaCl, 26 $NaHCO_3$, 11 glucose, 2.5 KCl, 1 NaH_2PO_4, 1.3 $MgSO_4$ and 2.5 $CaCl_2$. The slices were allowed to recover at 32°C for 30 min before being allowed to equilibrate at room temperature for a further 1 h. During recordings, the slices were placed in a recording chamber constantly perfused with heated ACSF (28-30°C) and gassed continuously with 95% O_2 and 5% CO_2.

For voltage clamp recordings, borosilicate glass pipettes (3-5 MΩ) were filled with an internal solution containing (in mM) 135 CsMeSO$_4$, 8 NaCl, 10 HEPES, 0.25 EGTA, 2 Mg$_2$ATP, 0.3 Na$_3$GTP, 0.1 spermine and 7 phosphocreatine (pH 7.25-7.3; osmolarity 294-298). Data was collected with a MultiClamp 700B amplifier (Axon Instruments) and digitized at 8 kHz using an ITC-18 A/D converter (Instrutech Corporation) and filtered at 4 KHz. Data were acquired using Axopatch (Molecular Devices) and analyzed using Axograph-X (Axograph).

DG granule cells were visually identified on an upright microscope (Olympus BX51WI, Olympus Optical) by infrared differential interference contrast. Theta glass pipettes filled with ACSF were used as a bipolar stimulation electrodes and were placed in the MPP and LPP. All excitatory synaptic recordings were made in the presence of picrotoxin (100 μM). Cells were held at -60 mV to record AMPAR EPSCs while stimulating afferent inputs at 0.1 Hz. NMDAR currents were calculated by measuring the amplitude of the dual component EPSC at +40 mV between 40 and 50 ms following the peak. NMDAR/AMPAR ratio of the EPSCs was calculated as the ratio of NMDAR EPSC at +40 mV and AMPAR EPSC at -60 mV. Paired pulse ratios were calculated as a ratio of the peak amplitudes of the EPSC-2 and EPSC-1 evoked by delivering two stimulations at an interval of 50 ms. To measure the input-output curves for MPP and LPP stimulation, 20-30 episodes of AMPAR EPSCs to incremental stimulus strength were measured for each pathway. LTP was induced by 2 trains of high frequency stimulation (100 Hz, 1 s) separated by 10 s, while cells were depolarized to 0 mV. This induction protocol was always applied within 10 min of achieving whole-cell configuration, to avoid "wash-out" of LTP. For LTP experiments, baseline and post-tetanus EPSCs were measured by delivering paired-pulses at an interval of 50ms. To generate summary graphs, individual experiments were normalized to the baseline and 6 consecutive responses were averaged to generate 1 minute bins. These were then averaged together to generate the final summary graphs. The magnitude of LTP was calculated based on the EPSC values 35-40 minutes after the end of the induction protocol. Normalized Change in paired pulse ratios following LTP were calculated as

$$(PPR\ [post\text{-}LTP]\text{- }PPR[pre\text{-}LTP])/(PPR[pre\text{-}LTP]).$$

RNA Fluorescent In-Situ Hybridization (FISH): RNA-FISH was performed as described previously (7). Briefly, wild-type C57/BL6 or CD-1 mice were euthanized with isofluorane at P30, followed by transcardial perfusion with ice cold PBS. The brain was quickly dissected and embedded in Optimal Cutting Temperature (OCT) solution on dry ice. Coronal and horizontal sections with 12-16 μm thickness were cut using Leica CM3050-S cryostat, mounted directly onto Superfrost Plus slides and stored at −80 °C until use. In-situ hybridization was performed using *Cbln4* probe (cat. no. 320269-C3) using the multiplex RNAscope platform (Advanced Cell Diagnostics) according to manufacturer instructions for fresh-frozen sections. Images were acquired using VS120 slide scanner (Olympus) at 20× magnification.

Quantitative Real Time (qRT) and Reverse Transcription (RT) PCR: Micro-dissected CA1 and DG tissues or whole cortex or kidneys were lysed in Trizol reagent (Thermo Fisher, 15596026) for RNA extraction following manufacturer's protocol. To measure relative *Neo1* and *Dcc* expression levels by qRT-PCR, following assay probes were used Neo1- Mm.PT.58.28686994 and Dcc-Mm.PT.58.7047849 (Integrated DNA Technologies). For RT–PCR to amplify alternatively spliced *Neo1* exons, total RNA (800-1000 ng) was used to synthesize cDNA using RT-PCR Kit (PrimeScript High Fidelity, R022A, Clontech). Following primers (5'-3') were used for Neo1 splice junction PCR amplification using synthesized cDNA; Neo1-SS1F- TCCAACTGTGAAGTGGGTCA, Neo1-SS1R – GATTGTCTCCATGAGGGTCT; Neo1-SS2-F – ACAATGTTGGCGAAGGCATC, Neo1-SS2-R – CACAGAGAACTCATAGAGCG; Neo1-SS3-F – AGTGAATTGGCAGCCTCCCT, Neo1-SS3-R – CAGAGACAATGATGACCAGC; Neo1-SS4-F – CCAGTGGACAATTCCATGGA, Neo1-SS4-R – ATGGTCAGTGCAGCACGTCT; Neo1-SS5-F-AGTCATCTCTACCACCCAAG, Neo1-SS5-R – TGGTGGTCTCCTGTACTTCA. Actb primers (F -TTGTTACCAACTGGGACGACA; R-TCGAAGTCTAGAGCAACATAGC) were used for control amplification. Amplicons were run on 1.5 or 2% agarose gel with GelRed gel dye (Biotium) and imaged using the ChemiDoc Gel Imaging station (Bio-Rad).

Plasmids: Full length Nrxn1-α-SS4+, Nrxn1-β-SS4+, *Cbln4* and *Dcc* coding sequences were cloned into pCDNA3.1 plasmids. HA tag sequence was N-terminally inserted after the signal peptide sequence of *Cbln4*. For *Nrxn1 and Dcc,* it was FLAG tag. pCMV5-Emerald (EmGFP)or pCMV5-DsRed expression plasmids were previously described (3).

Cloning of *Neo1* splice variants: cDNA (from CA3 and DG) encoding full-length *Neo1* was cloned into pcDNA3.1 expression plasmid with a FLAG sequence flanked by GSGS linker inserted after the signal peptide sequence. A total of 56 clones were sequenced using Sanger menthod using following primers to analyze the entire coding sequence of *Neo1*: (CMV-seq-F: AGTACATCAATGGGCGTGGA, Neo1-Seq1: GCAGAACAGCCAAGCTCACA, Neo1-Seq2: CTATCAATGCATTGCTGAGA, Neo1-Seq3: TCAACCACACAAAATGGGCA, Neo1-Seq4: CTATGAGTTCTCTGTGATGG, Neo1-Seq5: TGACTGATACTCCAATCCCT, Neo1-Seq6: TGAAGTACAGGAGACCACCA). The total number of clones containing a specific splice pattern was used to calculate the percentage of expression of *Neo1* splice variants.

Cell aggregation assay: Cell aggregation assay was performed as described before but modified to a 6-well format (3)**.** FreeStyle HEK293F cells (R79007, ThermoFisher) grown using FreeStyle 293 Expression Medium (12338018, ThermoFisher) to a density of 1×10^5 cells in a 3 mL volume per well of 6-well untreated tissue culture plate. Cells were co-transfected with 1 μg of either pCMV5-Emerald or pCMV5-DsRed and 1 μg of the indicated plasmid using a FreeStyle Max reagent (16447100, ThermoFisher). FreeStyle HEK293F cells were grown at 37°C/8%CO2 with shaking at 125 rpms for 48 hrs.

Depending on the combinations, transfected cells were mixed in non-coated 2 well plate at a 1:1 ratio and incubated for 2 hours with shaking. Mixed cells were allowed to settle and were imaged using a Nikon A1 confocal microscope with a 10x objective. To validate the expression of Flag and HA-containing constructs, immunocytochemistry was performed on HEK293F cells using anti-HA (mouse, Biolegend, MMS101R; 1:500) and anti-Flag (rabbit, Sigma, 7425; 1:500). Aggregation indices were calculated as previously described using ImageJ software (8).

Datasets: RNA in-situ hybridization data for *Neo1* was obtained from Allen Brain Atlas (http://mouse.brain-map.org/). To analyze the expression of 46 genes encoding presynaptic cell adhesion molecules in the mouse cortex and hippocampus, single-cell RNA-seq datasets were obtained from Allen Brain Map (https://portal.brain-map.org/atlases-and-data/rnaseq). Ensemble gene IDs manually entered and the Transcriptomic Explorer feature for Mouse "Whole Cortex & Hippocampus – 10X Genomics (2020) with 10X-SMART-Seq Taxonomy (2020)" was used to visualize the expression levels. For single-cell expression analysis of *Dcc* and *Neo1* in the DG, datasets from Linnarsson lab (L6_Dentate_gyrus_granule_neurons.loom) were analyzed. To visualize dentate granule cell clusters with relative Neo1 and Dcc expressions, Cell Scatterplot and Sparkline visualization features were used (http://loom.linnarssonlab.org/dataset/cellmetadata/Mousebrain.org.level6/L6_Dentate_gyrus_granule_neurons.loom).

Statistics: All data are presented as means ± SEMs. Statistical significance was calculated between the two genotypes using two-tailed t-tests (*p <0.05).
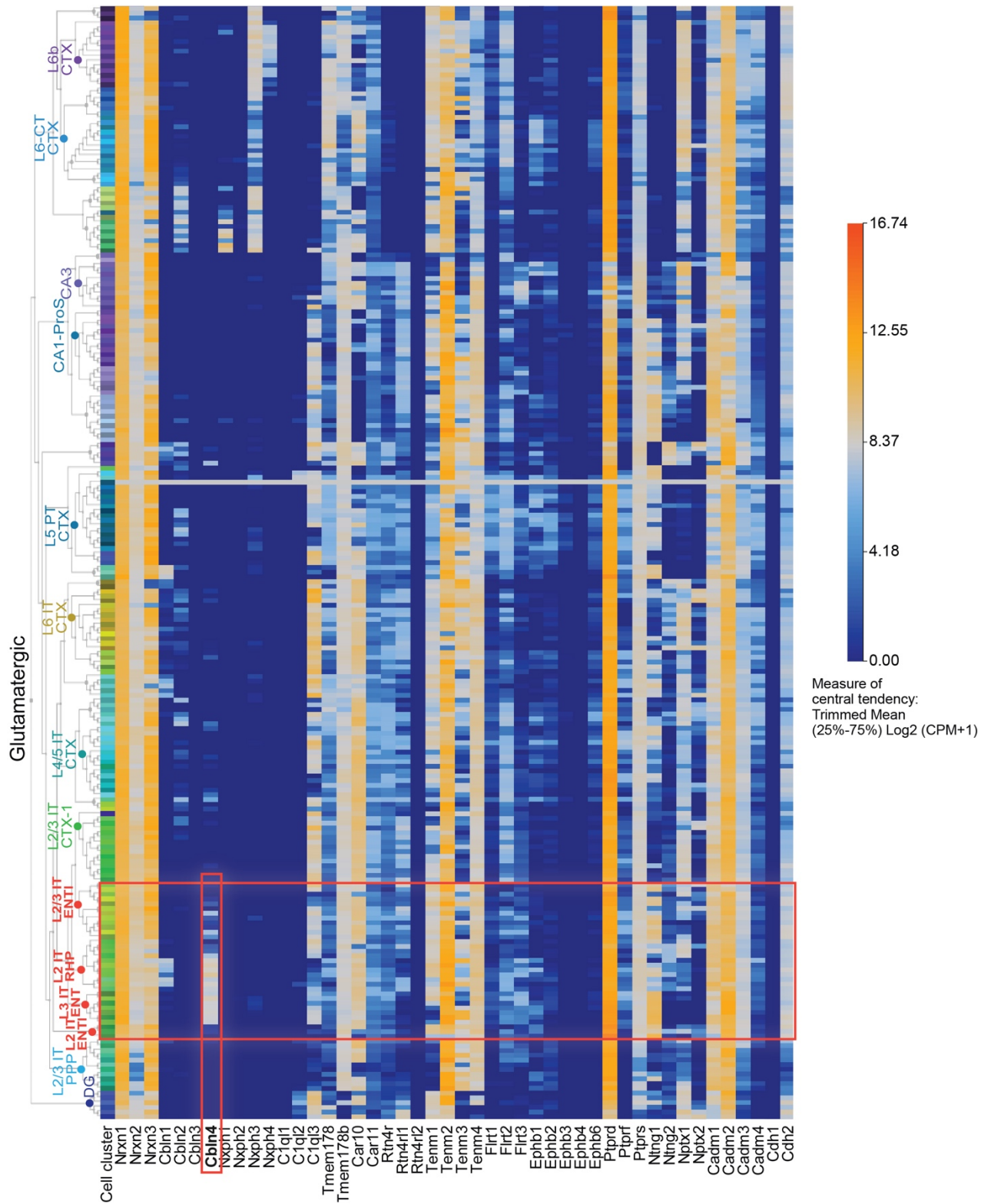
Figure S1. *Cbln4* **expression is highly enriched in the entorhinal cortex**

The image illustrates the mRNA expression levels of 46 presynaptic and secretory synaptic molecules in excitatory glutamatergic cell types revealed from single cell RNA-seq datasets obtained from the Allen Cell Types database. Note the high expression levels of *Cbln4* in layer 2/3 (L2/3) of the intratelencephalic (IT) lateral entorhinal (ENTl) and the retrohippocampal (RHP) area, which includes the lateral entorhinal and medial entorhinal areas (ENTm). Inhibitory and non-neuronal cell types are not shown. *Cbln4* and its enrichment in the entorhinal area are highlighted with orange boxes (abbreviations: CTX, cortex; PT, pyramidal tract; CA, Cornu Ammonis; ProS, prosubiculum; CT, corticothalamic neurons; PPP, pre-/post-/parasubiculum.
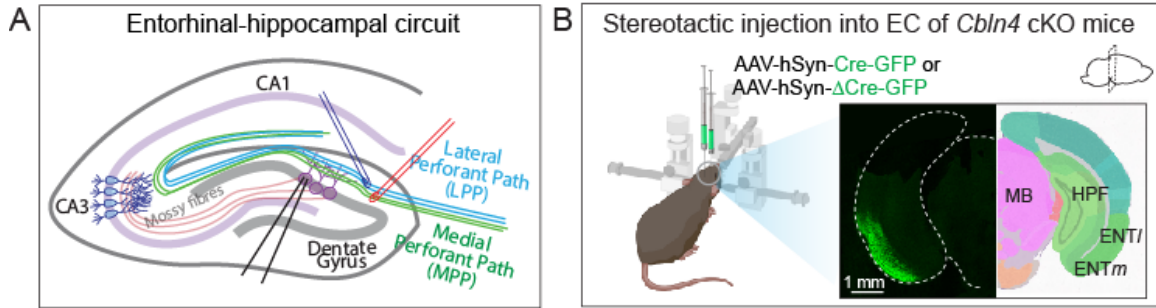
Figure S2. Schematic of the entorhinal cortex-hippocampal circuit and experimental approach to stereotactic injections into the entorhinal cortex (EC)

(A) Schematic of the hippocampal EC-DG circuit with electrode positions for electrophysiological stimulation of the MPP and LPP and for recordings from DG granule cells

(B) Schematic of stereotactic injections of AAVs into the EC of *Cbln4* cKO mice (left) and representative image and drawing of the injected brain section (right). AAVs used expressed Cre-eGFP or ΔCre-eGFP (control) driven by the human Synapsin-1 promoter.
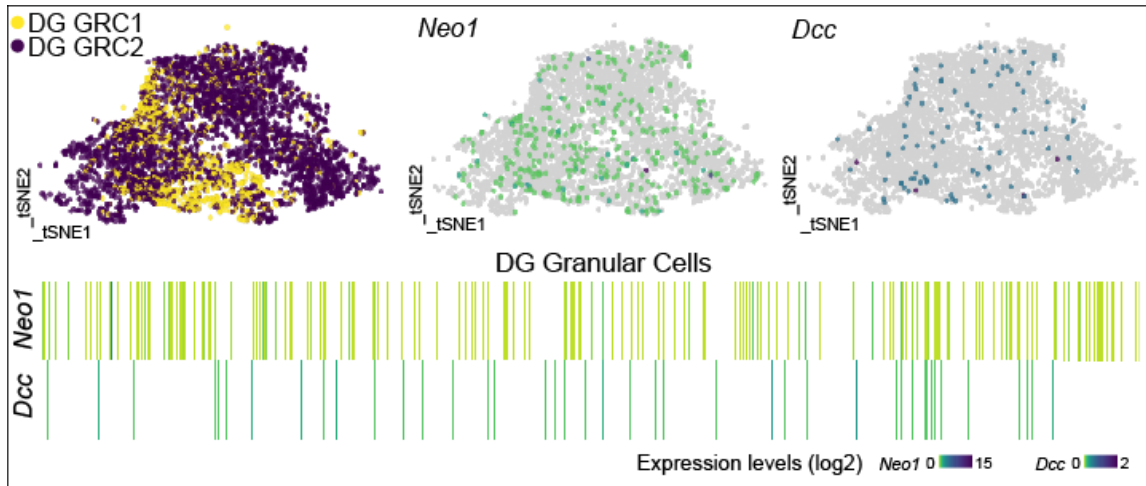
Figure S3. Single-cell RNA-seq data showing *Neo1* and *Dcc* expression in dentate gyrus granule cell populations.

tSNE plots (upper panels) of DG granule cell populations (GRC) and *Neo1* and *Dcc* expression in these two populations comprising 4368 single cells. Sparklines (lower panel) show expression level of *Neo1* and *Dcc* in corresponding cells. log2 expression values given.

Data were obtained from
http://loom.linnarssonlab.org/dataset/cellmetadata/Mousebrain.org.level6/L6_Dentate_gyrus_granule_neurons.loom. See ref (9).
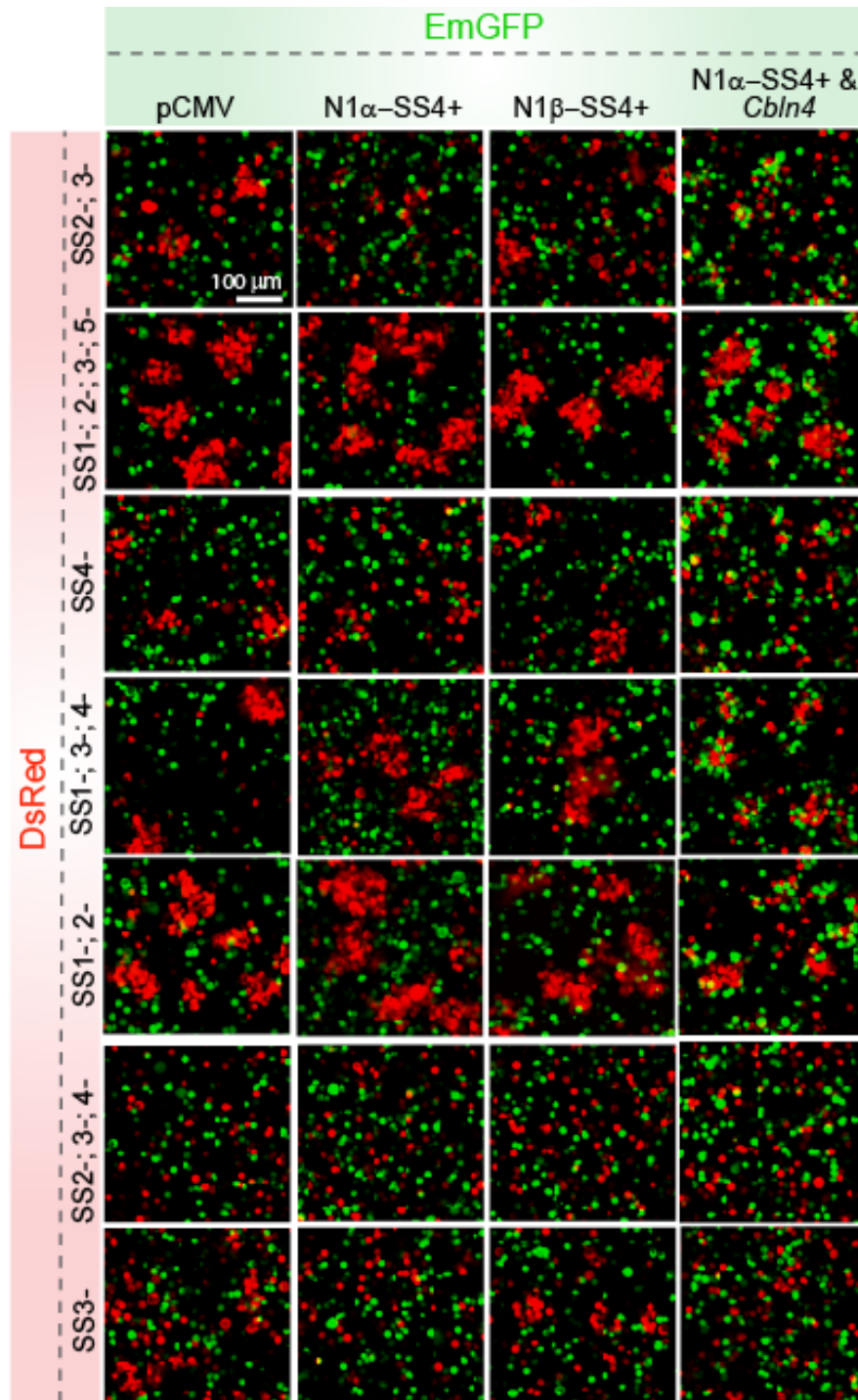
Figure S4. Cell-aggregation assays to validate Cbln4 interaction with Neo1 containing various splice sites

Confocal images of cell aggregation assay showing a strong aggregation of green cells (co-expressing EmGFP, N1a-SS4+ and *Cbln4*) with red cells (co-expressing DsRed and various *Neo1* splice variants or *Dcc*). Note that red cells expressing Neo1 splice variants exhibit a strong tendency to self-aggregate.
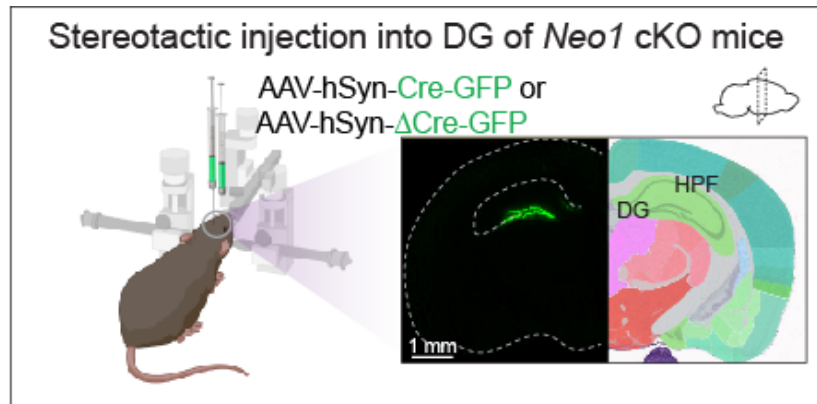
Figure S5. Schematic of stereotactic injections in *Neo1* cKO mice

Schematic and representative brain section of stereotactic injection of AAVs into the DG of *Neo1* cKO mice. AAVs used expressed Cre-eGFP or ΔCre-eGFP (control) driven by the human Synapsin-1 promoter.

SI References

1. Kam JW*, et al.* (2016) RGMB and neogenin control cell differentiation in the developing olfactory epithelium. *Development* 143(9):1534-1546.
2. Seigneur E & Sudhof TC (2017) Cerebellins are differentially expressed in selective subsets of neurons throughout the brain. *J Comp Neurol* 525(15):3286-3311.
3. Sando R, Jiang X, & Sudhof TC (2019) Latrophilin GPCRs direct synapse specificity by coincident binding of FLRTs and teneurins. *Science* 363(6429).
4. Masurkar AV*, et al.* (2017) Medial and Lateral Entorhinal Cortex Differentially Excite Deep versus Superficial CA1 Pyramidal Neurons. *Cell Rep* 18(1):148-160.
5. Beckervordersandforth R*, et al.* (2014) In vivo targeting of adult neural stem cells in the dentate gyrus by a split-cre approach. *Stem Cell Reports* 2(2):153-162.
6. Polepalli JS*, et al.* (2017) Modulation of excitation on parvalbumin interneurons by neuroligin-3 regulates the hippocampal network. *Nat Neurosci* 20(2):219-229.
7. Liakath-Ali K & Sudhof TC (2021) The Perils of Navigating Activity-Dependent Alternative Splicing of Neurexins. *Front Mol Neurosci* 14:659681.
8. Boucard AA, Maxeiner S, & Sudhof TC (2014) Latrophilins function as heterophilic cell-adhesion molecules by binding to teneurins: regulation by alternative splicing. *J Biol Chem* 289(1):387-402.
9. La Manno G*, et al.* (2021) Molecular architecture of the developing mouse brain. *Nature* 596(7870):92-96.